

Estimate the Effective Elastic Properties of Digitized Porous Rocks by Inverting the Cracks Unresolved

Yang Zhang and M. Nafi Toksöz

Earth Resources Laboratory
Dept. of Earth, Atmospheric and Planetary Sciences
Massachusetts Institute of Technology
Cambridge, MA 02139

Abstract

Current imaging technique such as micro X-ray CT can provide us detailed 3D micro-structures of porous rocks that can be used in numerical simulation so as to predict elastic properties of rocks saturated with different fluids. However, limited by the resolution the imaging process can provide, we usually lose the small features of rocks such as cracks and micro-pores, consequences of which can cause over-predicted effective elastic properties of porous rocks. In this paper, we present an inversion scheme to estimate the lost cracks during imaging process with Monte-Carlo algorithm. This method combines numerical simulation with theoretical models – the differential effective media model and Kuster-Toksöz model. Compared to the traditional inversion algorithms solely based on theoretical models, the algorithm presented in this paper utilizes the micro-structures of porous rocks resolved and takes the advantages of computational results from the digitized rocks, which in fact provides us much information of rocks and limits our inversion space for cracks. At end, we demonstrate the capability of this method on predicting the elastic properties of Berea sandstones measured in laboratory.

1. Introduction

In seismic data interpretation, understanding the relations between elastic properties of rocks, pore spaces and fluids is critical, expressions of which form the bases for reservoir characterization and monitoring. Effective properties of porous rocks highly depend on pore spaces, solid phases and interactions between these two. To accurately predict the properties of rocks requires highly precise information of its complex micro-structure and the ability of computationally solving the large 3D problems.

Traditionally, people formulate empirical relationships statistically from laboratory experiments to help predict properties of rocks (e.g., Wyllie et al., 1956; Wyllie et al., 1958; Han, 1986). However, such relationships are too simple to be predictive for a wide range of rocks, and lacks detailed description of micro-structure of rocks. Recently, the emergence of computational rock physics fills this gap and improves the research on rock physics (e.g., Roberts and Garboczi, 2000; Arns et al., 2002; Grechka and Kachanov, 2006; Saenger, 2008).

With current advanced imaging techniques such as micro-computed tomography (μ -CT), micro X-ray CT (Flannery et al., 1987; Spanne et al., 1994), focused ion beam scanning electron microscopy (FIBSEM), laser confocal microscopy (Fredrich et al., 1995), and magnetic resonance imaging (MRI), we now are able to generate 3D images of rocks in high resolution, the usual voxel resolution of which is about 2-10 μ m. Such high resolution images provide direct measurements of the complex morphology of porous rocks. Combining with computational techniques, we can calculate the material properties such as diffusivity, elasticity, permeability and conductivity. The ultimate goal of the development of these computational experiments and methods is to replace experiments having been traditionally carried out inside laboratories, which are time consuming and costly.

Two fundamental classes of numerical methods have been developed and used for studying rock properties. One consists of static methods, the other is dynamic method. Roberts and Garboczi (2000), Arns et al. (2002); Arns et al. (2007), Grechka and Kachanov (2006) and Madadi et al. (2009) used finite element method (FEM) to study the static effective elastic properties of porous media and rocks, while Saenger and Shapiro (2002); Saenger et al. (2004a); Saenger et al. (2004b); Saenger et al. (2005); Saenger et al. (2006); Saenger et al. (2007) and Saenger (2008) used finite difference method (FDM) to study the dynamic effective properties of porous and cracked rocks. Arns et al. (2002) carried out an extensive numerical computation on 3D digitized rocks of several Fontainebleau sandstones with variable porosities, and compared their numerical predictions to Gassmann's model and experimental measurements. They concluded that for such type of clean sandstone as Fontainebleau sandstone, elastic property-porosity relationships can be derived from microtomographic images. Arns et al. (2007) applied the same numerical method on the less well-cemented granular rocks, and studied the effects of contact moduli on linear effective elastic properties of such rocks. Saenger et al. (2000) developed a finite difference solver using rotated-staggered-grid scheme (RSG) and studied the dynamic responses of cracked rocks (Saenger and Shapiro, 2002; Saenger et al., 2004), in which he compared the numerical results to different effective medium theories. Saenger et al. (2005) extended the RSG scheme to incorporate the viscous effect of fluid into it and studied the Biot's effects of synthetic porous rocks. With the same solver, Saenger et al. (2006) and Saenger (2008) presented a new technique for static computations of effective elastic properties and explained discrepancies between some numerical studies in terms of static and dynamic numerical experiments. In all of these computations, they claimed the numerical predictions can verify some theoretical models, and even explain some experimental measurements, which is a good aspect of the computational experiment.

Though having the X-ray CT imaging technique nowadays, we are unable to obtain images of rocks with high enough resolution such that every single crack or micro-pore between and within grains for sandstones or carbonates can be illuminated. Even though we were able to do this, current computational resources should limit our ability to solve such huge 3D problems in a realistic scale since the resolution required has to be down to nanometer scale. Therefore, we generally lose small features of rocks during imaging process such as phase separation. Arns et al. (2007) realized this drawback of our current technique and tried to remedy it by introducing contact porosity for less well-cemented sandstones. In their approach, they utilized microtomographic images and grain-partitioning techniques to assign grain moduli, then used effective medium theories locally to calculate contact moduli between grains for phases such as clay.

However, we found that the loss of small features of rocks due to imaging process not only affects less well-cemented sandstones as Arns et al. (2007) discussed, but also for well-cemented sandstones such as Fontainebleau sandstones and Berea sandstones. For example, in the paper by Arns et al. (2002), though the numerical predictions with 3D digitized rocks of Fontainebleau sandstones using FEM can match Gassmann's equations and experimental measurements well, we found that (1) the computed velocities for both dry and water/oil saturated cases are generally higher than experimental measurements; (2) velocities

of P-wave for dry cases are higher than those for water/oil saturated cases, which contradicts the intuitions and laboratory observations for sandstones. We also found the same contradicting phenomena in our own computations on digitized 3D Berea sandstones. One explanation Arns (2002) gave to such observations is due to the periodical boundary condition used in the FEM solver. However, we do not think this is the real reason behind these observations. In this paper, we will discuss this problem and give an explanation to it first. Then we will propose a method to resolve this issue and finally calculate the effective elastic properties of rocks and compare these numerical predictions to laboratory measurements.

2. Overestimates of the Numerical Predictions

2.1 3D X-ray CT images of Berea sandstone

A 3D X-ray CT image for a cylindrical plug of Berea sandstone was obtained. The images have a total size of $1840 \times 1840 \times 1940$ with resolution of $2.8 \mu\text{m}$ per voxel. Gray scale images from X-ray CT have been thresholded so as to separate them into two main phases: solid grain and pore space, respectively. From the original cylindrical plug, we extracted a cubic subset in the center with the size of $250 \times 250 \times 250$ for analysis. In Figure 1, we show the gray scale CT images of the 250^3 cubic subset, and in Figure 2 we show the corresponding segmented images for this same subset, in which grains are represented in red and pores are in blue. The porosity (ϕ) of this sample is about 19.23%. As concluded by Arns et al. (2002), the representative image volume for well-cemented Fontainebleau sandstone should be 120^3 cubic subset at resolution of $5.7 \mu\text{m}$, which exactly corresponds to our sample with size of 250^3 at $2.8 \mu\text{m}$.

2.2 Properties predictions

We focus on the static effective properties of porous rocks as Arns et al. (2002) did on digitized 3D rock with finite element method (FEM). We use the finite element solver from NIST (National Institute of Standards and Technology) (Garboczi and Day, 1995; Garboczi, 1998) to estimate the effective elastic properties of Berea sandstone represented by the 250^3 cubic subset. FEM solves the weak form of the linear elastic equations and utilizes iterative solvers such as conjugate-gradient method to find the solutions. In FEM, each voxel is taken to be a trilinear finite element, and constant strain boundary conditions are applied. The effective elastic properties are obtained from average stresses and strains.

In the computation, we first assume the grains are occupied by pure quartz with bulk modulus $K=37$ GPa, shear modulus $\mu=44$ GPa and mineral density $\rho=2650$ kg/m^3 (Mavko et al., 1998). We model dry and water-saturated cases at 40 MPa pressure where $K_{\text{water}}=2.2$ GPa, $\mu_{\text{water}}=0$ GPa and $\rho_{\text{water}}=1000$ kg/m^3 (Han, 1986). The numerically predicted results for effective bulk $\langle K \rangle$ and shear $\langle \mu \rangle$ moduli and velocities of P- and S-wave are listed in Table 1. In Table 2, we list some laboratory measurements on Berea sandstones with similar porosities at 40 MPa as the one we used in this study for comparison where pulse-echo technique was employed to measure the velocities (Winkler, 1985; Han, 1986). At 40 MPa pressure, Winkler (1985) and Han (1986) both concluded that velocity dispersion due to fluids was so small as to be able to be ignored. Though the numerical predictions for dry, water-saturated cases satisfy Gassmann's

equation as Arns et al. (2002) demonstrated, we can see that the numerical predictions from FEM generally overestimate the effective elastic properties resulting in predicting large velocities in general, and also P-wave velocity predicted in water-saturated case is less than that for dry case, which usually happens only for well-sintered glass beads pack. This indicates that in our numerical computations, the bulk modulus of water contributes less to final effective properties but the effect of density takes over in the computation.

3. Issues with Imaging Process

The reason for overestimates of the numerical prediction is the loss of micro-structures of rocks in X-ray CT scanning and the image segmentation afterwards. As we know, small features like cracks or micro-pores in rocks are most in nanometer scale (Murphy et al., 1986). Though X-ray CT technique can provide us high resolution images in micrometer scale, compared to small features in nanometer scale, its resolution is still too low such that we can lose most information about these micro-structures when we digitize rocks into CT images and separate phases afterwards. Realizing these issues with imaging process, Arns et al. (2007) introduced the concept of contact porosity to estimate the contact moduli between grains with effective medium theories, and Knackstedt et al. (2009) utilized SEM images which have much higher resolution than CT images to recover micro-pores lost. For the samples of Berea sandstone we used in our study, we are facing the same issues as others do. Shown in Figure 3a is a 2D slice of X-ray CT image cut from the 3D volume of the digitized Berea sandstone. The arrows in Figure 3a indicate cracks between grain contacts that are lost during imaging process. As shown in Figure 3b, after segmentation, we obtain a rock with continuous matrix where no micro-structures between grains are resolved. As expected, the continuous matrix without cracks resulting from segmentation strengthens the rock frame and contributes to the over predicted effective elastic properties of digitized rocks. Though there should have other micro-structures as cracks lost in the imaging process, we only focus on cracks in our study since we believe they have the most impact on the effective elastic properties of rocks as discussed by many researchers already (e.g., Walsh, 1965; Kuster and Toksöz, 1974; O'Connell and Budiansky, 1977; Hudson, 1980).

4. Effects of Cracks on Digitized Rock Matrix

As discussed in the previous section, we believe that the loss of cracks between grains during imaging process is the main reason causing higher predicted effective elastic properties of rocks. Therefore, we have to modify the continuous matrix of digitized rocks so as to take the cracks into account. To accomplish this, effective medium theories are used along with computational approach. In section 2.2, we have calculated the velocities of P- and S-wave of Berea sandstone for dry and water-saturated cases based on the continuous rock matrix, which are much higher than the laboratory measurements. In order to recover cracks in the continuous matrix, we carry out a Monte-Carlo inversion on numerical predictions list in Table 1.

4.1 Effective medium theories

Note that instead of working on the continuous matrix directly to invert crack distribution, we start with the numerically predicted effective moduli of rocks first. According to differential effective medium theory (DEM), for a composite consisting of two phases, by choosing a preferred host material, we can incrementally add another phases or inclusions into the host. For the composite host medium at some porosity ϕ , the effective moduli $K^*(\phi + d\phi)$ and $\mu^*(\phi + d\phi)$ after a small portion of the composite host has been replaced by inclusions of the other phase can be obtained by

$$(1 - \phi) \frac{d}{d\phi} [K^*(\phi + d\phi)] = (K_i - K^*)P^*$$

$$(1 - \phi) \frac{d}{d\phi} [\mu^*(\phi + d\phi)] = (\mu_i - \mu^*)Q^*$$

where $K^*(\phi)$ and $\mu^*(\phi)$ are the effective moduli to be estimated after adding small portion of the second phase, K_i and μ_i are moduli of the second phase, and P^* and Q^* are geometric factors for inclusions of the second phase that depend on the shapes of inclusions (Berryman, 1992; Mavko et al., 1998).

Back to our cases, at beginning we treat pure quartz as the host that occupies the whole cubic domain without pores and cracks, and inclusions occupying the pore spaces resolved and cracks lost in the imaging process as the second phase to be added into the host of quartz. There are two ways of adding pores and cracks into host according to DEM. We can first add inclusions in pore spaces followed by those in cracks, or vice versa. Theoretically, the final effective elastic properties from such two sequences of adding the second phase can be quite different for some cases. The numerical predictions in Table 1 can be taken as the intermediate effective properties of rocks after only adding inclusions in pore spaces resolved. Therefore, starting with these results, we can invert distribution of cracks that should have existed in continuous matrix by using the Kuster-Toksöz model (Kuster and Toksöz, 1974).

4.2 Monte-Carlo inversion with the Kuster-Toksöz model

According to the DEM model, the numerical predictions listed in Table 1 can be thought of as the intermediate effective moduli of the Berea sandstone by only taking into account pores resolved from imaging process. Cracks lost in this process can be added into the continuous matrix as the rest portion of the second phase defined in the DEM model. Taking the saturated Berea sandstone in the intermediate stage of DEM model as an isotropic and homogeneous elastic block, and using the Kuster-Toksöz model (Kuster and Toksöz, 1974), we can study the effects of cracks on final effective moduli of this porous Berea sandstone.

Combing the Kuster-Toksöz model with the Monte-Carlo inversion, we can invert distributions of spheroidal cracks assumed in the Kuster-Toksöz model by fitting laboratory measurements. For the laboratory data, we choose only those for dry and water-saturated cases in Table 2 measured by Han (1986). Since the laboratory data were measured at 40 MPa pressure, we believe most cracks with smaller aspect ratio ($<10^{-5}$) are closed by pressure (Toksöz et al., 1976). Therefore, in the Monte-Carlo inversion, we choose 4 sets of cracks with initial aspect ratios α_0 and maximum concentrations c_{\max} , respectively.

$$\alpha_0 = [(5 \pm 2.5) \times 10^{-2}, (1 \pm 0.5) \times 10^{-2}, (5 \pm 2.5) \times 10^{-3}, (1 \pm 0.5) \times 10^{-3}]$$

$$c_{\max} = [5 \times 10^{-2}, 5 \times 10^{-3}, 1 \times 10^{-4}, 1 \times 10^{-5}]$$

Note that we allow the values of aspect ratio corresponding to each set of crack to vary within some specific range as defined above. We totally ran 100 Monte-Carlo inversions, in each of which 100000 trials were computed. We use L_2 -norm to measure the error between computed P- and S-wave velocities for dry and water-saturated cases and laboratory measurements. The best set of cracks with minimum error was chosen out of these 100 best solutions as the final inverted result. Listed in Table 3 are the best solutions for aspect ratio and concentration of cracks and their mean and standard deviation after inversion. We can see that adding small amount of cracks, especially those with small aspect ratios, can affect the elastic properties of rocks significantly.

Adding the inverted set of cracks into Berea sandstone in the intermediate stage according to the DEM and Kuster-Toksöz models, we can obtain the final P- and S-wave velocities for dry: $V_p=3957.3$ m/s, $V_s=2646.5$ m/s; water: $V_p=4118.8$ m/s, $V_s=2600.0$ m/s, which are close to laboratory measurements by Han (1986).

4.3 Numerical predictions for cracked digitized matrix

So far we have discussed the effects of cracks lost on the effective properties of porous medium from computational approach, and inverted a set of cracks with laboratory measurements based on the DEM and Kuster-Toksöz models. To carry out computations on digitized rocks by taking cracks lost into account, alternatively we have to first add cracks into quartz to obtain a continuous matrix but being softened by cracks and inclusions. Then we saturate pore spaces resolved in imaging process and compute the total effective elastic properties at end. This sequence of adding inclusions or second phase is opposite to what we did in section 4.2. According to the DEM model, the effective properties of composite are generally different depending on the sequence of adding different inclusions, but in some cases they can be quite close.

Saturating the cracks inverted in previous section 4.2 with dry, water, brine and oil, and adding them into quartz by using Kuster-Toksöz models, we can obtain the effective elastic properties of new continuous matrix as listed in Table 4. Here we choose properties for brine: $K_{\text{brine}}=2.51$ GPa, $\mu_{\text{brine}}=0$ GPa and

$\rho_{\text{brine}}=1040 \text{ kg/m}^3$; oil: $K_{\text{oil}}=2.16 \text{ GPa}$, $\mu_{\text{oil}}=0 \text{ GPa}$ and $\rho_{\text{oil}}=890 \text{ kg/m}^3$ (Winkler, 1985). Since Berea sandstone is not as clear as Fontainebleau sandstone, saturating brine can change micro-structures of pore spaces in term of changes in clay. So we reduce 5% of the shear modulus of quartz when saturating brine so as to take into account the effect of clay (Toksöz et al., 1976).

Assigning the values of effective elastic properties in Table 4 to solid grains of the 3D digitized Berea sandstone shown in red in Figure 2, and using the FEM solver to compute the final effective properties for cases saturated with corresponding inclusions, we can obtain the final results listed in Table 5 where we put the computed results side by side with laboratory measurements of Winkler (1985) and Han (1986) for comparison. The values in percentage below each laboratory data are errors between computed velocities and corresponding laboratory measurements. We can see from these small errors that (1) our newly predicted effective properties match laboratory measurements quite well for all four cases; (2) since we inverted the distribution of cracks only with laboratory measurements by Han (1986) for dry and water-saturated cases, the good match between computed results for these two cases and measurements should be within expectation, which also indicates that the different sequences of adding inclusions defined by DEM model does not lead to much discrepancy of results in our cases; (3) importantly, by adding cracks inverted from dry and water-saturated cases based on measurements by Han (1986), we can predict the effective properties of brine and oil-saturated rocks well enough to match measurements in laboratory (Winkler, 1985). In Figure 4, we conclude the procedure employed here to invert cracks and then predict effective elastic properties of rocks by taking these cracks into account. Note that the rock we use here has porosity of 19.23%, and we think the inverted results can only apply to rocks with such similar porosity.

5. Conclusions

In this paper, we present an inversion scheme to estimate the lost cracks in micro X-ray CT imaging process, which combines numerical simulation and theoretical models - the differential effective media model and Kuster-Toksöz model. By including the cracks into the original matrix, we can numerically predict the elastic properties of Berea sandstones quite well compared to laboratory measurements. This algorithm utilizes the micro-structures of porous rocks resolved in imaging process and takes the advantages of computational results from such digitized rocks, which is an improvement compared to the traditional inversion algorithms solely based on theoretical models.

Acknowledgement

The authors would like to thank Schlumberger-Doll Research for funding the Canonical Rock Physics project and providing the digitized rock data. Yang Zhang also would like to thank ERL Funding Member Consortium for support.

References

- CH Arns. *The influence of morphology on physical properties of reservoir rocks*. PhD thesis, University of New South Wales, Sydney, Australia, 2002.
- CH Arns, MA Knackstedt, WV Pinczewski, and EJ Garboczi. *Computation of linear elastic properties from microtomographic images: Methodology and agreement between theory and experiment*. Geophysics, 67(5):1396_1405, SEP-OCT 2002.
- CH Arns, M Madadi, AP Sheppard, and MA Knachstedt. *Linear elastic properties of granular rocks derived from X-ray CT images*. SEG Expanded Abstract, 1711_1714, 2007.
- JG Berryman. *Single-scattering approximations for coefficients in Biot equations of poroelasticity*. Journal of the Acoustical Society of America, 91(2):551_571, FEB 1992.
- BP Flannery, HW Deckman, WG Roberge, and KL Damico. *3-D X-ray microtomography*. Science, 237(4821):1439_1444, SEP 18 1987.
- JT Fredrich, B Menendez, and TF Wong. *Imaging the pore structure of geomaterials*. Science, 268(5208):276_279, APR 14 1995.
- EJ Garboczi. *Finite element and finite difference programs for computing the linear elastic and linear electric properties of digital images of random materials*. Technical report, National Institute of Standards and Technology, 1998.
- EJ Garboczi and AR Day. *Algorithm for computing the effective linear elastic properties of heterogeneous materials - 3-D results for composites with equal phase Poisson ratios*. Journal of the Mechanics and Physics of Solids, 43(9):1349_1362, SEP 1995.
- V Grechka and M Kachanov. *Effective elasticity of rocks with closely spaced and intersecting cracks*. Geophysics, 71(3):D85_D91, 2006.
- DH Han. *Effects of porosity and clay content on acoustic properties of sandstones and unconsolidated sediments*: Ph.D. thesis. PhD thesis, Stanford University, 1986.
- JA Hudson. *Overall properties of a cracked solid*. Mathematical Proceedings of the Cambridge Philosophical Society, 88(SEP):371_384, 1980.
- MA. Knackstedt, S Latham, M Madadi, A Sheppard, T Varslot, and CH Arns. *Digital rock physics: 3D imaging of core material and correlations to acoustic and flow properties*. The Leading Edge, 28(1):28_33, 2009.
- GT Kuster and MN Toksöz. *Velocity and attenuation of seismic-waves in two-phase media: Part I. Theoretical formulation*. Geophysics, 39(5):587_606, 1974.

- M Madadi, AC Jones, CH Arns, and MA Knackstedt. *3D imaging and simulation of elastic properties of porous materials*. Computing in Science & Engineering, 11(4): 65_73, JUL-AUG 2009.
- G Mavko, T Mukerji, and J Dvorkin. *The rock physics handbook*. Cambridge University Press, 1998.
- WF Murphy, KW Winkler, and RL Kleinberg. *Acoustic relaxation in sedimentary rocks: Dependence on grain contacts and fluid saturation*. Geophysics, 51(3):757_766, 1986.
- RJ O'Connell and B Budiansky. *Viscoelastic properties of fluid-saturated cracked solids*. Journal of Geophysical Research, 82(36):5719_5735, 1977.
- AP Roberts and EJ Garboczi. *Elastic properties of model porous ceramics*. Journal of the American Ceramic Society, 83(12):3041_3048, DEC 2000.
- EH Saenger and SA Shapiro. *Effective velocities in fractured media: a numerical study using the rotated staggered finite difference grid*. Geophysical Prospecting, 50(2):183_194, MAR 2002.
- EH Saenger, N Gold, and SA Shapiro. *Modeling the propagation of elastic waves using a modified finite-difference grid*. Wave Motion, 31(1):77_92, JAN 2000.
- EH Saenger, OS Kruger, and SA Shapiro. *Effective elastic properties of randomly fractured soils: 3D numerical experiments*. Geophysical Prospecting, 52(3):183_195, MAY 2004a.
- EH Saenger, OS Kruger, and SA Shapiro. *Numerical considerations of fluid effects on wave propagation: Influence of the tortuosity*. Geophysical Research Letters, 31 (21), NOV 13 2004b.
- EH Saenger, SA Shapiro, and Y Keehm. *Seismic effects of viscous Biot-coupling: Finite difference simulations on micro-scale*. Geophysical Research Letters, 32(14): L14310, JUL 26 2005.
- EH Saenger, OS Krueger, and SA Shapiro. *Effective elastic properties of fractured rocks: Dynamic vs. static considerations*. International Journal of Fracture, 139 (3-4):569_576, JUN 2006.
- EH. Saenger, R Ciz, OS Krueger, SM Schmalholz, B Gurevich, and SA Shapiro. *Finite-difference modeling of wave propagation on microscale: A snapshot of the work in progress*. Geophysics, 72(5, Suppl. S):SM293_SM300, SEP-OCT 2007.
- Erik H. Saenger. *Numerical methods to determine effective elastic properties*. International Journal of Engineering Science, 46(6):598_605, JUN 2008.
- P Spanne, JF Thovert, CJ Jacquin, WB Lindquist, KW Jones, and PM Adler. *Synchrotron computed microtomography of porous media - Topology and transports*. Physical Review Letters, 73(14):2001_2004, OCT 3 1994.
- MN Toksöz, CH Cheng, and A Timur. *Velocities of seismic waves in porous rocks*. Geophysics, 41(4):621_645, 1976.
- JB Walsh. *Effect of cracks on the compressibility of rock*. Journal of Geophysical Research, 70(2):381_389, 1965.

KW Winkler. *Dispersion analysis of velocity and attenuation in Berea sandstone*. Journal of Geophysical Research, 90(NB8):6793_6800, 1985.

MRJ Wyllie, AR Gregory, and LW Gardner. *Elastic wave velocities in heterogeneous and porous media*. Geophysics, 21(1):41_70, 1956.

MRJWyllie, AR Gregory, and GHF Gardner. *An experimental investigation of factors affecting elastic wave velocities in porous media*. Geophysics, 23(3):459_493, 1958.

Table 1: Numerical predictions from finite element method for the digitized Berea sandstone.

	$\langle K \rangle$ (GPa)	$\langle \mu \rangle$ (GPa)	V_p (m/s)	V_s (m/s)
Dry	20.598	20.268	4717.4	3677.6
Water	22.974	20.556	4640.0	2963.8

Table 2: Laboratory measurements of velocities on Berea sandstones with similar porosities at 40 MPa (Winkler, 1985; Han, 1986). (unit: m/s)

	porosity (ϕ)	Dry		Water		Brine		Oil	
		V_p	V_s	V_p	V_s	V_p	V_s	V_p	V_s
Han (1986)	20.3	4040	2620	4150	2510				
Winkler (1985)	19.03	3963	2527			4044	2417	4189	2521

Table 3: The set of cracks from Monte-Carlo inversion at 40 MPa.

	Aspect Ratio (α)
Best Solution	$[6.62 \times 10^{-2}, 1.36 \times 10^{-2}, 3.13 \times 10^{-3}, 9.09 \times 10^{-4}]$
Mean	$[7.20 \times 10^{-2}, 1.34 \times 10^{-2}, 5.51 \times 10^{-3}, 1.05 \times 10^{-3}]$
Standard Derivation	$[2.39 \times 10^{-3}, 1.59 \times 10^{-3}, 1.35 \times 10^{-3}, 2.84 \times 10^{-4}]$
	Concentration (c)
Best Solution	$[4.50 \times 10^{-2}, 1.30 \times 10^{-3}, 3.26 \times 10^{-5}, 5.01 \times 10^{-6}]$
Mean	$[4.98 \times 10^{-2}, 8.08 \times 10^{-4}, 3.93 \times 10^{-5}, 2.92 \times 10^{-6}]$
Standard Derivation	$[1.83 \times 10^{-4}, 3.13 \times 10^{-4}, 2.83 \times 10^{-5}, 2.02 \times 10^{-6}]$

Table 4: Effective elastic properties of continuous matrix with cracks included at 40 MPa.

	$\langle K \rangle$ (GPa)	$\langle \mu \rangle$ (GPa)
Dry	24.086	30.265
Water	28.608	31.627
Brine	28.868	30.268
Oil	28.556	31.612

Table 5: Final effective properties of the 3D digitized Berea sandstone for cases saturated with different inclusions at 40 MPa. (unit: m/s)

	<K> (GPa)	< μ > (GPa)	Computed		Han (1986)		Winkler (1985)	
			V _p	V _s	V _p	V _s	V _p	V _s
Dry	13.578	13.883	3988.6	2623.5	4040	2620	3963	2527
					-1.27%	0.13%	0.65%	3.81%
Water	17.796	14.889	4085.1	2569.0	4150	2521		
					-1.56%	1.9%		
Brine	18.075	14.338	4051.8	2515.7			4044	2417
							0.19%	4.08%
Oil	17.736	14.877	4105.0	2583.1			4189	2521
							-2.01%	2.46%

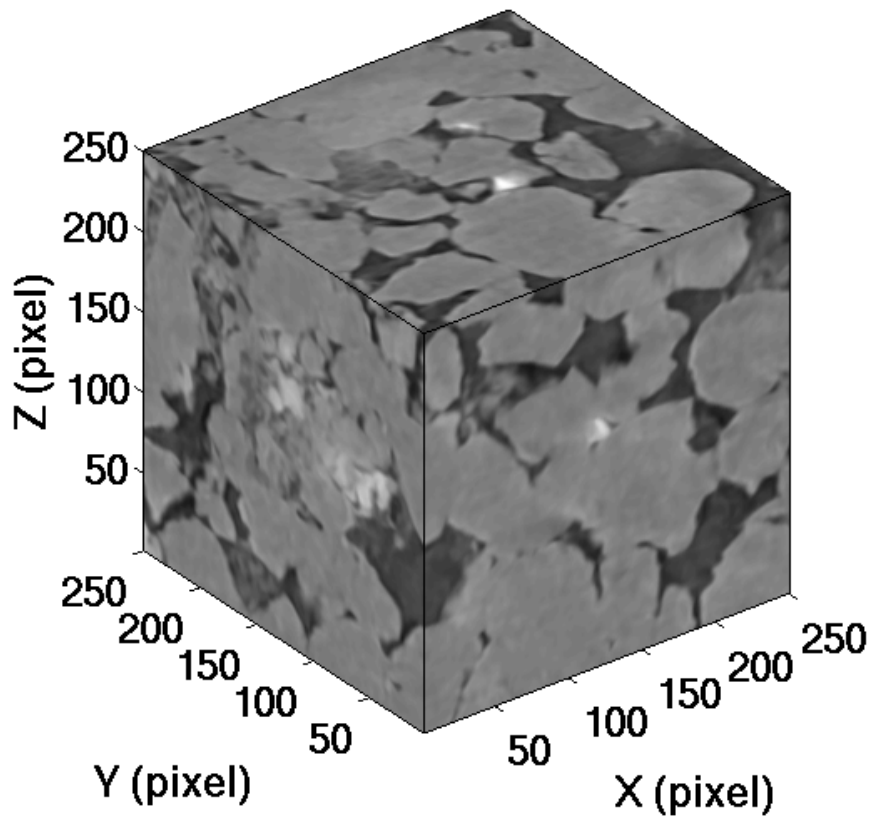


Figure 1: Gray scale X-ray CT images for the 250^3 cubic subset of a Berea sandstone.

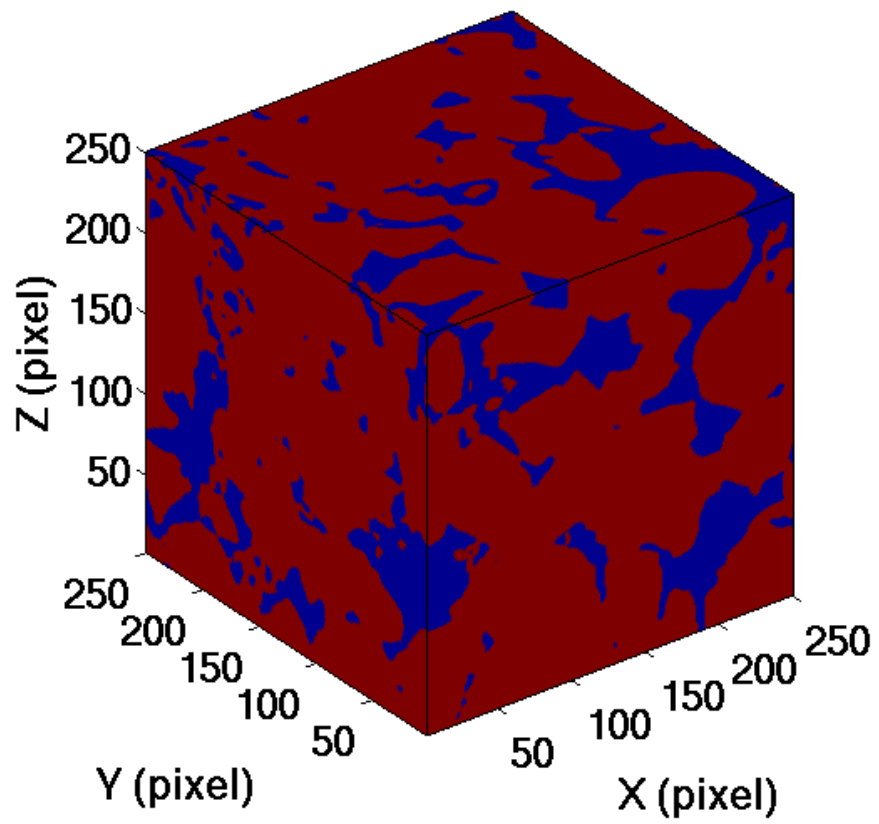


Figure 2: Segmented images for the 250^3 cubic subset of a Berea sandstone. Grains are presented in red and pores are in blue.

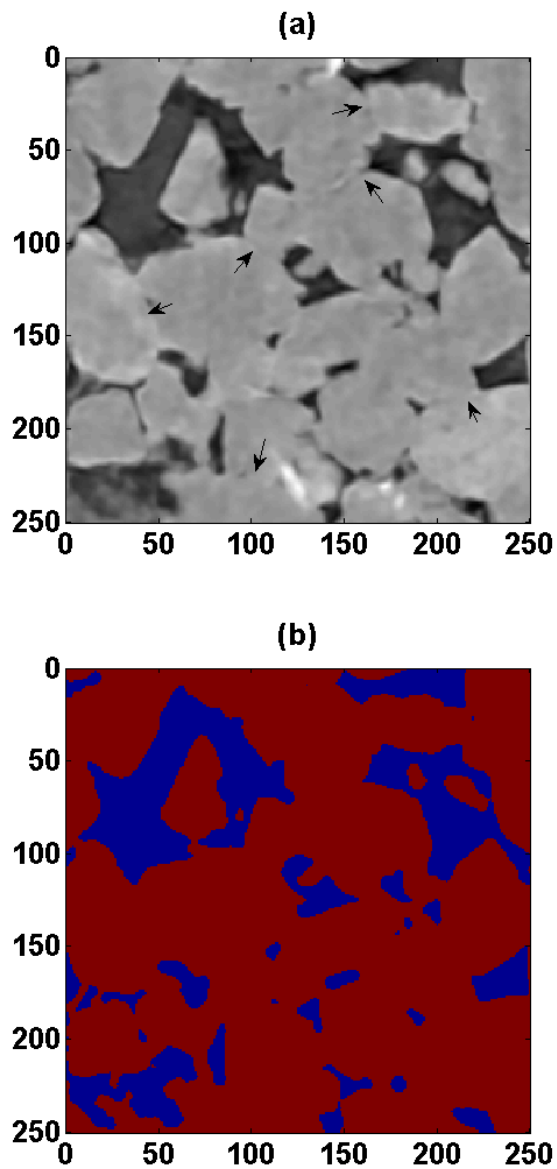


Figure 3: 2D slices of digitized Berea sandstone. (a) X-ray CT image in gray scale; (b) segmented image. We can clearly see the loss of cracks between grain contacts due to imaging process, as indicated by arrows in (a).

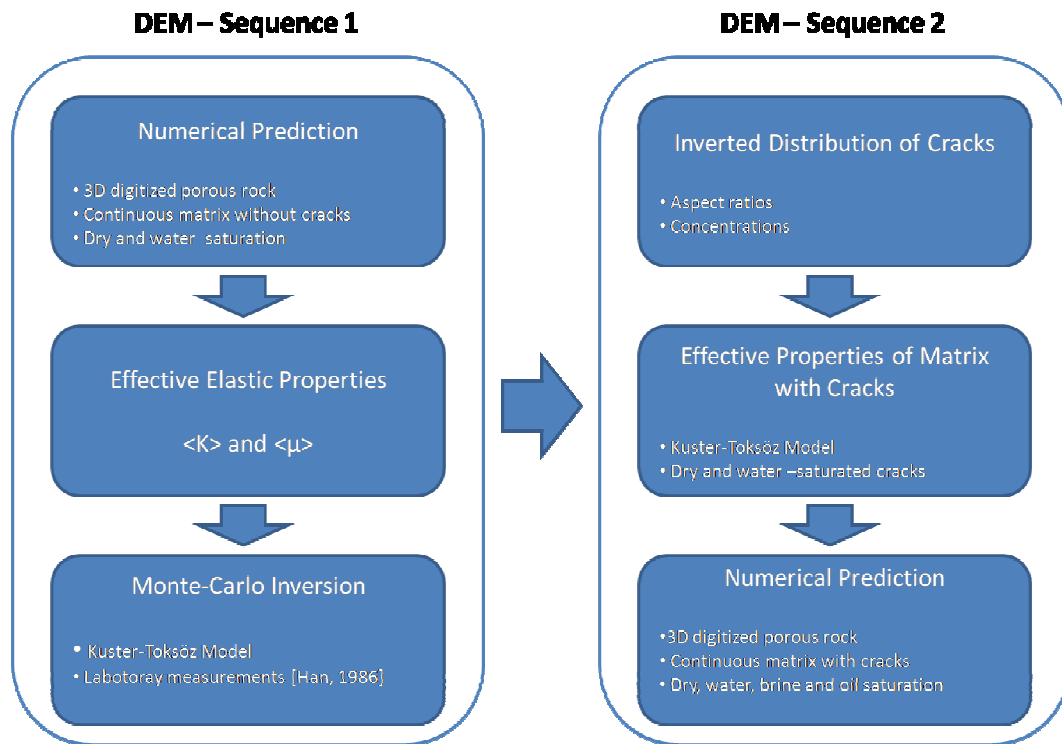


Figure 4: Flow chart for procedures to predict effective elastic properties of 3D digitized porous rock with cracked matrix.